

# Identifying resonances with wave-packet dynamics

Alexis Diaz-Torres and Jeffrey A. Tostevin

*Department of Physics, University of Surrey, Guildford GU2 7XH, UK*

(Dated: February 14, 2019)

## Abstract

A new method for the study of resonant behavior - using wave-packet dynamics - is presented, based on the powerful window operator technique. The method is illustrated and quantified by application to the astrophysically-important example of low-energy  $^{12}\text{C} + ^{12}\text{C}$  collisions. For this selected, potential model test case, the technique is shown to provide both resonance energies and widths in agreement with alternative methods, such as complex-energy scattering-matrix pole searches and scattering phase-shift analyses. The method has a more general capability to study resonance phenomena across disciplines, that involve particles temporarily trapped by potential pockets.

PACS numbers:

## I. INTRODUCTION

Resonance phenomena, where particles are temporarily trapped by attractive potential pockets, are ubiquitous in many fields of physics, chemistry, molecular biology and technology. For instance, shape-type or potential resonances appear in resonance tunneling in quantum wells and quantum wires [1] as well as in the rapid neutron-capture process that is crucial for heavy element creation in the Universe [2].

To describe such resonance phenomena quantitatively, various methods have been developed using Hermitian and non-Hermitian quantum mechanics. These methods include the location of poles of the scattering matrix (S-matrix) in the complex energy plane, analysis of the density of states spectra, the asymptotes of continuum eigenfunctions, the scattering phase shifts, complex scaling methods, and filter diagonalization methods. These methods are comprehensively reviewed in Ref. [3]. Resonances can also be determined by analytic continuation of eigenvalues from the stabilization graph into the complex energy plane [4] and by using wave-packet dynamics [5].

The present paper provides a new method for describing potential resonances, using wave-packet dynamics [6–8] along with the powerful window operator method [10]. As a topical test case, and so as to allow direct, quantitative comparisons with alternative techniques, we use a simplified potential model dynamical description of  $^{12}\text{C} + ^{12}\text{C}$  nuclear collisions at bombarding energies near to the Coulomb barrier. The results of the present method can be compared directly with those obtained using complex energy plane S-matrix pole searches and analyses of the scattering phase shifts [11]. We note that many of the alternative methods, mentioned above, will actually be more efficient in determining such potential resonances in the test case of the present paper. However, the one-dimensional potential model of  $^{12}\text{C} + ^{12}\text{C}$  collisions allows illustration of the key ideas of the proposed method that describes resonances dynamically. More generally, in the physical description of nuclear collisions and reactions, for instance the fission and fusion of heavy ions, an understanding of the dynamical formation and decay of intermediate (nuclear molecular) structures is crucial [8, 12–14]. Usually, multi-dimensional potential pockets support these short-lived structures, whose description in terms of stationary-state methods is challenging as the boundary conditions are unclear. In such contexts, the present method is useful. Here, we present both a description of the model problem and a critical evaluation of the

proposed method and its results, followed by a summary.

## II. MODEL AND METHODS

### A. General aspects of the time-dependent wave-packet method

The time-dependent wave-packet method involves three steps [6–8]:

- (i) the definition of the initial wave function  $\Psi(t = 0)$ ,
- (ii) the propagation  $\Psi(0) \rightarrow \Psi(t)$ , dictated by the time evolution operator,  $\exp(-i\hat{H}t/\hbar)$ , where  $\hat{H}$  is the total Hamiltonian that is time-independent,
- (iii) the calculation of observables (e.g., spectra) from the time-dependent wave function,  $\Psi(t)$ .

The wave function and the Hamiltonian are represented in a grid. In the present work, for simplicity, these are considered a function of only the internuclear distance,  $R$ .

### B. The Hamiltonian

The Hamiltonian,  $\hat{H} = \hat{T} + \hat{V}$ , is formed by the radial kinetic energy operator,  $\hat{T} = -\frac{\hbar^2}{2\mu} \frac{\partial^2}{\partial R^2}$ , and a real total potential energy,  $\hat{V} = \frac{\hbar^2 J(J+1)}{2\mu R^2} + U(R)$ , which includes a centrifugal component with a total angular momentum  $J$ . Here  $\mu$  denotes the reduced mass and  $U(R)$  is comprised of the nuclear and Coulomb interactions. Fig. 1 shows the real total potentials for  $^{12}\text{C} + ^{12}\text{C}$  for the  $J = 0, 2, 4$  partial waves, as calculated in Ref. [8]. These potentials were determined by folding the collective potential-energy landscape (including the centrifugal energy) of non-axial symmetric di-nuclear configurations with the probability density of the ground-state wave-function of the two deformed, colliding  $^{12}\text{C}$  nuclei [9]. The heights of the Coulomb barriers are 6.5 MeV ( $J = 0$ ), 6.8 MeV ( $J = 2$ ), and 7.6 MeV ( $J = 4$ ) and their radii are 8 fm, 7.9 fm and 7.8 fm, respectively. Resonance states are formed in the attractive pockets of these potentials, as is shown below.

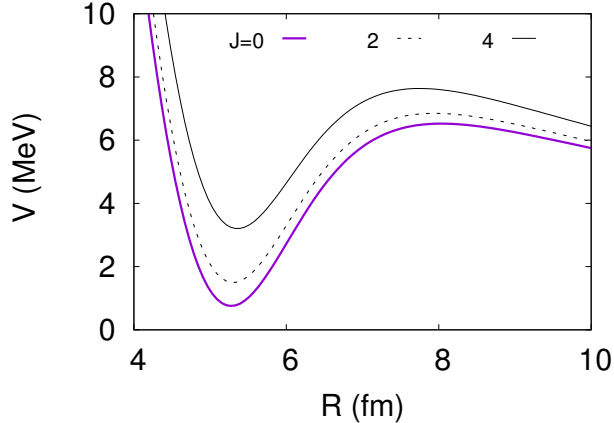


FIG. 1: (Color online) Real  $^{12}\text{C} + ^{12}\text{C}$  total potentials for the  $J = 0, 2, 4$  partial waves [9].

### C. Initial wave function and time propagation

The initial wave function,  $\Psi_0(R)$ , is described by a Gaussian wave-packet, centered at a large internuclear distance  $R_0$  and having a spatial width  $\sigma$ . This initial wave-packet is boosted toward the potential barriers, shown in Fig. 1, with an average wave-number  $K_0$  appropriate to the kinetic energy for the mean total incident energy  $E_0$ . That is,

$$\Psi_0(R) = \frac{1}{\pi^{1/4}\sqrt{\sigma}} \exp\left[-\frac{(R - R_0)^2}{2\sigma^2}\right] e^{-iK_0(R - R_0)}. \quad (1)$$

In the following calculations, an initial wave-packet with  $R_0 = 400$  fm,  $\sigma = 10$  fm and the mean total incident energy around the heights of the Coulomb barriers,  $E_0 = 6$  MeV, is assumed. These parameters do not affect the resonance energies calculated [7], provided (i) the initial wave-packet is fully contained in the position and wave-number grids, (ii) its amplitude at the grid edges is negligible, and (iii) the initial position  $R_0$  is larger than the classical turning points for wave-numbers in the interval  $(-K_0 \pm 3/\sigma)$ . The wave-packet is represented on a Fourier radial grid [15]:  $R = 0 - 1000$  fm with 2048 evenly spaced points.

The time propagation of the wave function was carried out using the Chebyshev propagator [15] for the evolution operator, as is described in Appendix C of Ref. [8]. In this work the time-step used was  $\Delta t = 10^{-22}$  s, for which the normalization of the wave function is preserved with an accuracy of  $\sim 10^{-14}$ . As was stated above, for the sake of simplicity and for ease of comparisons with alternative methods, other dynamical processes, such as inelastic scattering of the  $^{12}\text{C}$  nuclei, are neglected. The initial and time-evolved wave-packets contain a range of translational energies, so the calculation of observables requires an energy

projection method.

#### D. The energy projection method

Within the window operator approach, the energy spectrum of a time-dependent numerical wave function,  $|\Psi\rangle$ , is  $\mathcal{P}(E_k) = \langle\Psi|\hat{\Delta}|\Psi\rangle$ , where  $\hat{\Delta}$  is the window operator with centroid energy  $E_k$  [10]:

$$\hat{\Delta}(E_k, n, \epsilon) \equiv \frac{\epsilon^{2n}}{(\hat{H} - E_k)^{2n} + \epsilon^{2n}}. \quad (2)$$

Here,  $\hat{H}$  is the system Hamiltonian, and  $n$  determines the shape of the window function.  $\mathcal{P}(E_k)$  represents the probability of finding the system, in state  $|\Psi\rangle$ , in the energy window  $E_k \pm \epsilon$ . As  $n$  is increased, the shape of the window function rapidly becomes rectangular with very little overlap between adjacent energy bins with centroid energies  $E_k$ , the bin width remaining constant at  $2\epsilon$  [10]. The spectrum is constructed for a set of  $E_k$  where  $E_{k+1} = E_k + 2\epsilon$ . In this work,  $n = 2$  and  $\epsilon$  will be specified in each of the calculations below. Solving two successive linear equations for the vectors  $|\chi_k\rangle$ :

$$(\hat{H} - E_k + \sqrt{i}\epsilon)(\hat{H} - E_k - \sqrt{i}\epsilon)|\chi_k\rangle = \epsilon^2|\Psi\rangle, \quad (3)$$

yields  $\mathcal{P}(E_k) = \langle\chi_k|\chi_k\rangle$ . Thus, the vectors  $|\chi_k\rangle$  represent bin states over the energy range  $E_k \pm \epsilon$ .

#### E. Potential resonances from wave-packet dynamics

The key idea of the present method for determining resonances from wave-packet dynamics is to calculate the energy spectrum of that part of  $|\Psi\rangle$  that is inside the radius of the  $J$ -dependent Coulomb barriers in Fig. 1. This part, denoted  $|\tilde{\Psi}\rangle$ , is first normalized to unity, and Eq. (3) is then solved using  $|\tilde{\Psi}\rangle$  in the source term. At any given time, the *effective* spectrum is:

$$\mathcal{P}(E_k) \equiv \frac{\langle\tilde{\Psi}|\hat{\Delta}|\tilde{\Psi}\rangle}{\langle\Psi_0|\hat{\Delta}|\Psi_0\rangle}. \quad (4)$$

The denominator here, the energy spectrum of the initial wave-packet, displayed in Fig. 2, is employed to remove the dependence on the relative weights of incident energies in the initial wave-packet. The effective spectrum is normalized to unity, revealing structures

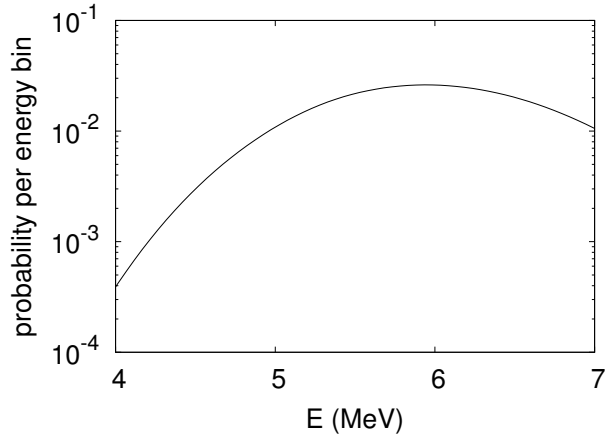


FIG. 2: The energy spectrum of the initial wave-packet with  $E_0 = 6$  MeV. The bin width is  $2\epsilon = 50$  keV and the maximum radius of the grid is  $R_{max} = 1000$  fm.

due to potential resonances. This deduced spectrum converges very quickly as the body of the recoiling wave-packet moves away from the potential pocket, and long before that body approaches the external edge of the radial grid. Hence, the  $|\tilde{\Psi}\rangle$  is not contaminated by waves reflected at the external edge of the grid, else a complex absorbing potential would have to be used at that edge. However, the bin states  $|\chi_k\rangle$  of Eq. (3) are subject to the boundary condition due to the finite extent,  $R_{max}$ , of the numerical grid of the one-dimensional radial box. The discrete representation of the radial kinetic energy operator uses Eq. (A8) of Ref. [16]. Fig. 3 shows the normalized resonant bin state, for  $J = 0$  and  $E_k = 4.43$  MeV, when the position,  $\mathcal{R}$ , of the body of the recoiling wave-packet is at  $\mathcal{R} = 25$  fm. The radial probability density of this bin state inside the radius of the Coulomb barrier (arrow) is essentially the same for grids with  $R_{max} = 1000$  and 3000 fm, while the (small) amplitude of the long-range oscillatory behavior reduces significantly as the grid is extended. This resonant bin state also approaches the scattering state obtained by direct integration of the time-independent Schrödinger equation (TISE), the thick solid line in Fig. 3, as the grid is extended, indicating that the  $|\chi_k\rangle$  approximate the continuum of scattering states.

### III. RESULTS

Figure 4 shows the effective energy spectra of the part of the time-dependent wave-packet, with  $E_0 = 6$  MeV and a given  $J$ , that is inside the radius of the Coulomb barriers

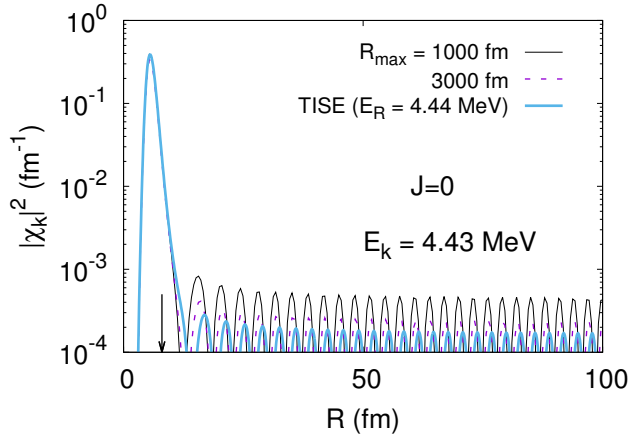


FIG. 3: (Color online) The radial probability density of a normalized resonant bin state from Eq. (3), for  $E_k = 4.43$  MeV and  $\epsilon = 1$  keV, using grids with  $R_{max} = 1000$  and  $3000$  fm. The part,  $|\tilde{\Psi}\rangle$ , of the time-dependent wave-packet,  $|\Psi\rangle$ , that is inside the radius of the  $J = 0$  Coulomb barrier (arrow) in Fig. 1, is used in the source term of Eq. (3). The position of the body of the recoiling  $|\Psi\rangle$ , with  $E_0 = 6$  MeV, is at  $\mathcal{R} = 25$  fm. The resonant bin state from Eq. (3), with extended grids, approaches the resonant, continuum-scattering state obtained by direct integration of the time-independent Schrödinger equation (TISE), indicating that  $|\chi_k\rangle$  correctly approximate the continuum scattering states.

of Fig. 1. Three resonant structures are clearly visible in these spectra, whose strengths converge rapidly as the position of the body of the recoiling wave-packet moves away from the Coulomb barrier region and the non-resonant energy backgrounds in this internal region gradually decline.

Figure 5 displays, on a linear scale, a probability density function that results from dividing a highly resolved effective spectrum by the bin width, i.e.,  $\mathcal{P}(E_k)/2\epsilon$ . Here the bin widths are  $2\epsilon = 2$  keV and the wave-packet position is  $\mathcal{R} = 25$  fm.

There are two intrinsic energies/resolutions of importance in the numerical calculations. The first is the chosen bin parameter,  $\epsilon$ , of the window operator in Eq. (2). The second is the spectral resolution of the wave function calculation, the separation  $\Delta E$  between continuum eigenstates of the Hamiltonian imposed by the finite spatial extent,  $R_{max}$ , of the numerical grid used. This spectral resolution can be increased, i.e.  $\Delta E$  reduced, to examine narrow resonances, by transferring the numerical wave functions  $|\Psi_0\rangle$  and  $|\tilde{\Psi}\rangle$  in Eq. (4), to a larger grid with the same grid point spacing [10]. The transferred wave functions are assumed to

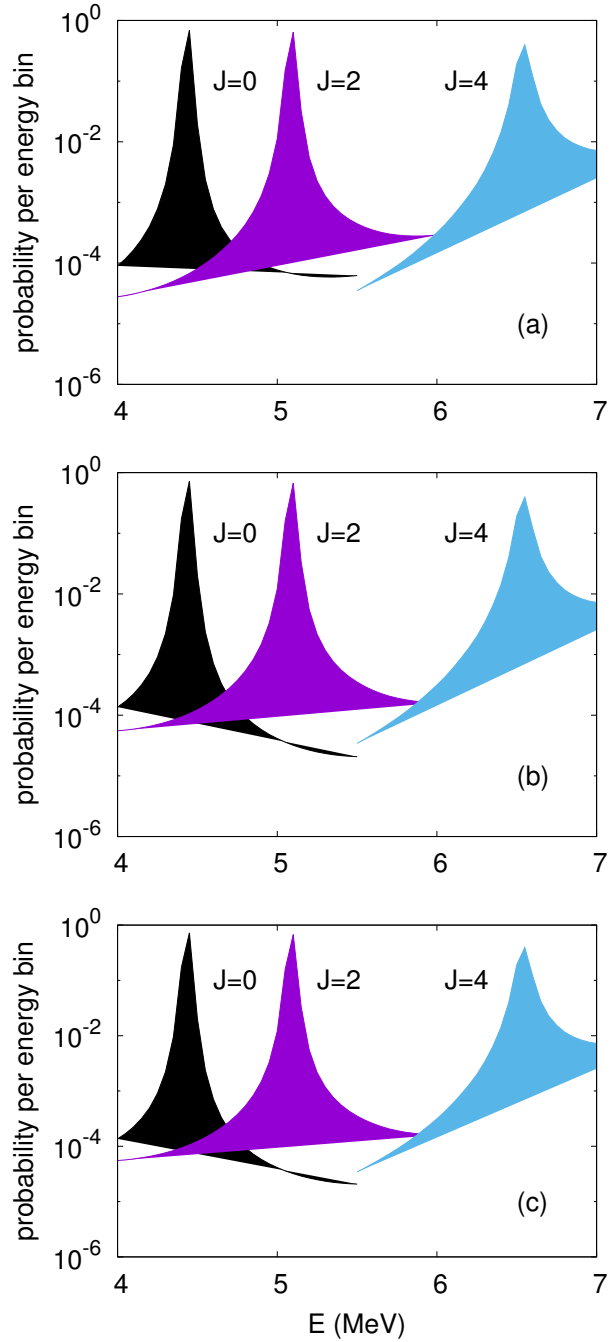


FIG. 4: (Color online) Effective energy spectra for the part of the time-dependent wave function inside the radius of the corresponding Coulomb barriers in Fig. 1. The bin width is  $2\epsilon = 50$  keV and the maximum radius of the grid is  $R_{max} = 1000$  fm. Three instances are shown, when the position  $\mathcal{R}$  of the body of the recoiling wave-packet, with  $E_0 = 6$  MeV, is: (a) near the distance of minimal approach, (b) is at  $\mathcal{R} = 25$  fm, and (c) is at  $\mathcal{R} = 50$  fm. The strength of these resonances converges rapidly as the recoiling wave-packet moves away from the Coulomb barriers.

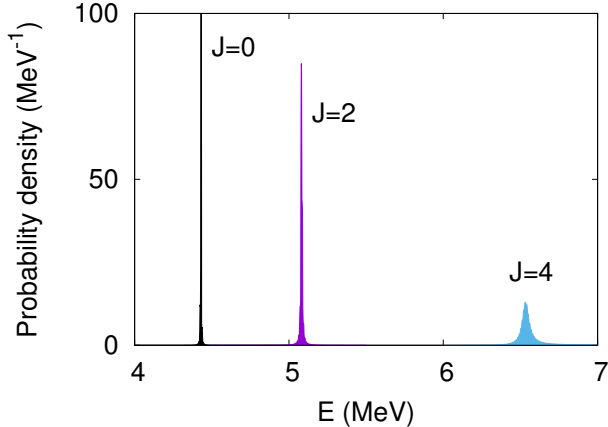


FIG. 5: (Color online) Probability density function,  $\mathcal{P}(E_k)/2\epsilon$ , for bins of  $2\epsilon = 2$  keV and  $\mathcal{R} = 25$  fm. The maximum radius of the grid is  $R_{max} = 3000$  fm.

vanish for radii beyond the original grid. The optimal  $R_{max}$  should ideally be such that the spacing  $\Delta E$  between continuum eigenstates is smaller or of the same order as both the bin width,  $2\epsilon$  and the resonance widths of interest. If not, the computed spectrum reveals artifacts (step-like structures) due to the limited resolution [10]. A reasonable lower bound on  $\Delta E$  in the present case is obtained assuming free-particle propagation. Since the total potentials involved are less than 0.1 MeV for  $R \gtrsim 500$  fm, neighboring eigenstates, for a given  $R_{max}$ , approximately satisfy  $\Delta K R_{max} = \pi$ , with the result that  $\Delta E \approx (E/K)(2\pi/R_{max})$ , with  $E = \hbar^2 K^2/2\mu$ . So, for  $R_{max} = 3000$  fm and  $E \approx 4$  MeV,  $\Delta E \gtrsim 8$  keV.

This expected improvement in the  $\Delta E$  resolution with increasing  $R_{max}$  can be observed in Fig. 6(c) that presents the probability density for  $J = 4$  using three different grid extents (symbols),  $R_{max} = 1000, 3000$  and  $7000$  fm. Figures. 6(a) and 6(b) show this dependence of the probability density on the grid size for the narrower  $J = 0$  and  $J = 2$  resonances, respectively, and the expected improved quality of the probability density function when increasing the grid size from  $R_{max} = 3000$  to  $7000$  fm.

Fitting the isolated, narrow peaks in Fig. 6 to a normalized Lorentzian:

$$f(E, E_R, \Gamma_R) = \frac{1}{\pi} \frac{\Gamma_R/2}{(E - E_R)^2 + (\Gamma_R/2)^2}, \quad (5)$$

both the resonance energies,  $E_R$ , and their widths,  $\Gamma_R$ , can be extracted. This is carried out using the nonlinear least-squares Levenberg-Marquardt algorithm [17, 18] implemented in the *gnuplot* package. Fig. 6 shows the Lorentzian (solid line) that fits the probability

density for each partial wave, using the grid with  $R_{max} = 7000$  fm (solid circles). For fitting lineshapes of overlapping, broad resonances, the Padé approximant method [4] can be used to determine  $E_R$  and  $\Gamma_R$ .

These fitted  $E_R$  and  $\Gamma_R$  values are presented in Table I for grids with  $R_{max} = 3000$  and  $7000$  fm. Also shown are the values calculated using a complex-energy S-matrix pole search and from the scattering phase shifts [11]. The phase shift function,  $\delta(E)$ , for the three partial waves, is displayed in Fig. 7 and the associated resonance widths were determined using the formula,  $\Gamma_R = 2(d\delta(E)/dE|_{E_R})^{-1}$  [3], that provides accurate widths for narrow, isolated resonances [3]. Evident from Fig. 7 is that, in the present case, the resonances occur in the presence of significant background phases. Comparing the results of the present method to those from the S-matrix poles approach, in Table I, we note that the resonance energy centroids are in excellent agreement (all to better than 1%), while there is a disagreement ( $\sim 1$  keV for  $J = 0$  and 2) in the widths of the narrower resonances, using the grid with  $R_{max} = 3000$  fm. The latter can be improved by using more extended grids, as demonstrated for the grid with  $R_{max} = 7000$  fm. The mapped Fourier method for non-uniform grids [19] can improve the efficiency of the present approach. Overall, the present method provides a reliable means to locate and quantify the potential resonances. The resonances calculated in the present study account for some resonant structures observed in the astrophysical S-factor for stellar carbon burning [8].

TABLE I: Resonance energies (MeV) and their widths (keV), extracted from Fig. 6 for  $R_{max} = 3000$  and  $7000$  fm, are compared to those from the S-matrix pole search and scattering phase shift methods. While the absolute errors of all  $E_R$  from the present method are  $< 0.01\%$ , those for  $\Gamma_R$  are between 0.5 and 6%.

$J$	present method		S-matrix poles		phase shifts	
	$E_R$	$\Gamma_R$	$E_R$	$\Gamma_R$	$E_R$	$\Gamma_R$
	$R_{max} = 3000$ (7000) fm					
0	4.430 (4.431)	$2.75 \pm 0.09$ ( $1.10 \pm 0.07$ )	4.437	1.55	4.437	1.58
2	5.081 (5.082)	$6.62 \pm 0.15$ ( $5.91 \pm 0.29$ )	5.088	5.70	5.089	6.14
4	6.535 (6.535)	$49.62 \pm 0.23$ ( $49.72 \pm 0.30$ )	6.538	49.50	6.555	73.85

## IV. SUMMARY

In summary, a new method for studying resonance phenomena using wave-packet dynamics has been presented, based on the powerful window operator method. We demonstrate, in the case of the astrophysically-important, low-energy  $^{12}\text{C} + ^{12}\text{C}$  system, that the method calculates resonance energies and widths in agreement with alternative, established methods. The present, dynamical technique is more generally applicable for the quantitative study of resonance phenomena in different fields, where particles are temporarily trapped by attractive potential pockets.

### Acknowledgments

The support from the STFC grant (ST/P005314/1) is acknowledged. A.D-T is very thankful to the ECT\* in Trento, where some of the calculations were carried out, for their support during a research visit in August 2018. We thank Prof. Nimrod Moiseyev for constructive comments.

- 
- [1] S. Bhattacharyya et al., *Nature Materials* **5**, 19 (2006).
  - [2] C. Rolfs and W.S. Rodney, *Cauldrons in the Cosmos* (University of Chicago Press, Chicago, 1988) p. 449.
  - [3] N. Moiseyev, *Non-Hermitian Quantum Mechanics* (Cambridge University Press, Cambridge, United Kingdom, 2011) p. 41.
  - [4] I. Haritan and N. Moiseyev, *J. Chem. Phys.* **147**, 014101 (2017).
  - [5] T. Goldzak, I. Gilary and N. Moiseyev, *Mol. Phys.* **110**, 537 (2012).
  - [6] D.J. Tannor, *Introduction to Quantum Mechanics: A Time-Dependent Perspective* (University Science Books, Sausalito, 2007) p. 273.
  - [7] M. Boselli and A. Diaz-Torres, *Phys. Rev. C* **92**, 044610 (2015).
  - [8] A. Diaz-Torres and M. Wiescher, *Phys. Rev. C* **97**, 055802 (2018).
  - [9] See Supplemental Material at <http://link.aps.org/supplemental/10.1103/yyy.zz.xxxxxx> for numerical values of the total potentials shown in Fig. 1.

- [10] K.J. Schafer and K.C. Kulander, Phys. Rev. A **42**, 5794 (1990); K.J. Schafer, Comp. Phys. Comm. **63**, 427 (1991).
- [11] E. Merzbacher, *Quantum Mechanics* (Third Edition, John Wiley & Sons, Inc., New York, 1998) p. 302.
- [12] A. Tumino et al., Nature **557**, 687 (2018).
- [13] P.D. Goldstone et al., Phys. Rev. C **18**, 1706 (1978).
- [14] A. Tudora, F.-J. Hambsch and S. Oberstedt, Nucl. Phys. A **890**, 77 (2012).
- [15] R. Kosloff, Ann. Rev. Phys. Chem. **45**, 145 (1994).
- [16] D.T. Colbert and W.H. Miller, J. Chem. Phys. **96**, 1982 (1992).
- [17] K. Levenberg, Quart. Appl. Math. **2**, 164 (1944).
- [18] D. Marquardt, J. Soc. Indust. Appl. Math. **11** (2), 431 (1963).
- [19] M. Nest and H.-D. Meyer, Chem. Phys. Lett. **352**, 486 (2002).

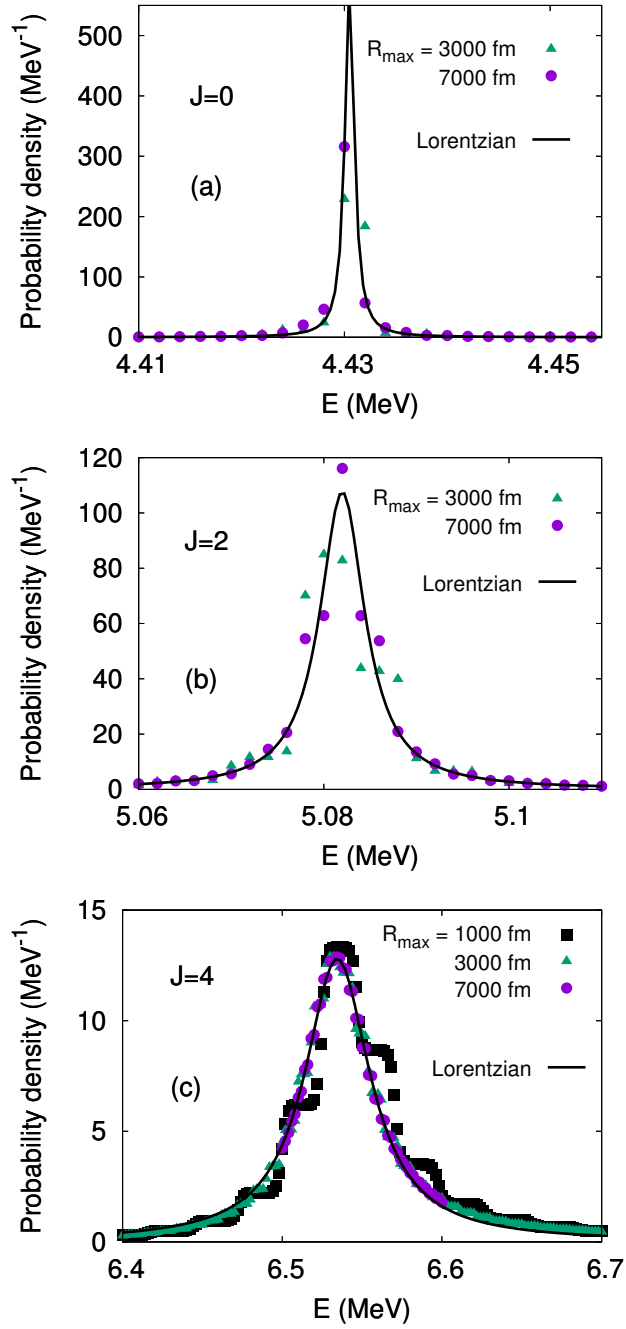


FIG. 6: (Color online) The same as Fig. (5), using various extended grids (symbols), for (a)  $J = 0$ , (b)  $J = 2$ , and (c)  $J = 4$ . The Lorentzian curves (solid lines) were fitted to the calculated strength functions for the grid with  $R_{max} = 7000$  fm (solid circles).

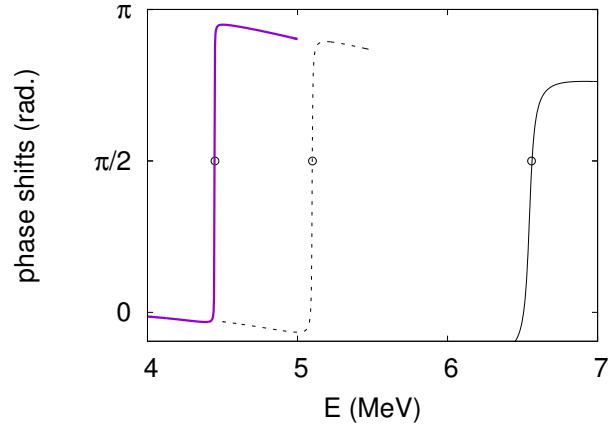


FIG. 7: (Color online) The scattering phase shifts for the potentials shown in Fig. 1. The small circles denote the resonance energies, taken as  $\delta(E_R) = \pi/2$ , with values  $E_R = 4.44$  MeV ( $J = 0$ ), 5.09 MeV ( $J = 2$ ) and 6.56 MeV ( $J = 4$ ).